Implementation of a Flexible and Modular Multiphase Framework for the Analysis of Surface-Tension-Driven Flows Based on a Hybrid LS-VOF Approach

Paolo Capobianchi, Marcello Lappa and Mónica S. N. Oliveira

Abstract The mathematical modelling and numerical simulation of multiphase flows are both demanding and highly complex. In typical problems with industrial relevance, the fluids are often in non-isothermal conditions, and interfacial phenomena are a relevant part of the problem. A number of effects resulting from the presence of temperature differences must be adequately taken into account to make the results of numerical simulations consistent and realistic. Moreover, in general, gradients of surface tension at the interface separating two liquids are a source of numerical issues that can delay (and in some circumstances even prevent) the convergence of the solution algorithm. Here, we propose a fundamental and concerted approach for the simulation of the typical dynamics resulting from the presence of a dispersed phase in an external matrix under non-isothermal conditions based on the modular computer-aided design, modelling and simulation capabilities of the OpenFOAM® environment. The resulting framework is tested against the migration of a droplet induced by thermocapillary effects in the absence of gravity. The simulations are fully three-dimensional and based on an adaptive mesh refinement (AMR) strategy. We describe in detail the countermeasures taken to circumvent the problematic issues associated with the simulation of this kind of flow.

1 Introduction

The motion of gas bubbles and liquid droplets in fluid media is a widespread phenomenon in nature and a subject of great relevance to many engineering and material processing applications.

A fluid particle can move under the influence of different driving forces of a distinct nature. As an example, a falling raindrop or a bubble rising in a denser liquid are put in motion because of the gravity force exerted on it by Earth. Other body forces

P. Capobianchi (✉) · M. Lappa · M. S. N. Oliveira
James Weir Fluids Laboratory, Department of Mechanical and Aerospace Engineering, University of Strathclyde, Glasgow G1 1XJ, UK
e-mail: paolo.capobianchi@strath.ac.uk

J. M. Nóbrega and H. Jasak (eds.), *OpenFOAM®* ,
https://doi.org/10.1007/978-3-319-60846-4_18

such as magnetic and ultrasonic fields can also be used to induce or "control" the motion of droplets in some specific circumstances (see, for instance, [7, 16]). Even in the absence of body forces, a similar phenomenon can be induced by another fundamental mechanism, the so-called *thermal Marangoni* (or *thermocapillary*) *effect*. This process, which occurs every time a gradient of temperature or concentration is present at the interface separating two fluid phases, becomes particularly important in all of those situations in which body forces (such as gravity) do not play a major role, e.g., in the microgravity environment provided by orbiting platforms, or when either the densities of the fluid pair are similar and/or the typical size of the dispersed phase is very *small* (e.g., atomised droplets).

The first pioneering study on the thermocapillary migration of droplets was conducted in the late 50s by Young et al. [26], who, under some limiting assumptions (perfectly spherical drop of radius R moving in an infinitely extended fluid domain under Stokes flow conditions), derived a landmark solution (in analytical form) of the governing equations. With such an approach, velocity and temperature fields were considered to be fully established at every moment of time, while neglecting the inertia and convective effects. Under this approximation, the temperature field can be inferred independently of the flow field, and this greatly simplifies the derivation of an analytical solution to the problem, yielding a precise relationship between the asymptotic (steady) droplet migration velocity and the properties of the considered fluids and characteristics of the driving force.

Over subsequent years, especially because of the advent of space programs and the possibility of executing experiments in the field of fluids and materials in space (sounding rockets, Space Shuttle, and most recently, the International Space Station, see, e.g., [12]), the subject gained increasing popularity, extending to multidisciplinary fields.

Balasubramaniam and Subramanian [2] extended the analytical study of Young et al. [26] to the case in which the Reynolds number tends to infinity. They analysed the steady migration of a spherical drop in a continuous phase when subjected to a temperature gradient under conditions such that inertial terms in the momentum equation and convective-transport terms in the energy equation dominate over the corresponding molecular-transport terms (i.e., $Ma \to \infty$ and $Re \to \infty$, for which they were able to derive analytical solutions partially based on the earlier mathematical model of Harper and Moore [11]). The migration velocity of the drop was obtained by these authors in the framework of a potential-flow theory by equating the rate at which work is done by the thermocapillary stress to the rate of viscous dissipation of energy; the method of matched asymptotic expansions was employed to solve the conjugate heat-transfer problem in the two phases (characterised by the presence of thin thermal boundary layers both outside and within the drop). In physical terms, they found that in the limit of $Ma \to \infty$, the velocity of a drop is proportional to the square of the temperature gradient and the cube of the radius of the drop, whereas in the opposite limit ($Ma \to 0$), both dependencies are linear.

In addition to theoretical studies, a number of experimental works have also appeared over the last two decades (see, e.g., [3, 9, 23] for experiments under weightless conditions). More recently, attempts have been made to approach the

problem directly in the framework of moving boundary methods such as Volume of Fluid (VOF) or Level Set (LS) techniques, by which the typical simplifications of past analytical approaches can be removed and the typical difficulties (and cost) of microgravity-based experimentation avoided.

Despite valuable numerical advances over the years [6, 10, 13, 15, 21, 25, 27], the numerical simulation of droplets migrating under the influence of surface-tension gradients at finite values of the Reynolds and Marangoni numbers can still be regarded as an "open task". In the present chapter, we lay the general foundation of a possible theoretical and mathematical treatment of the subject based on the modular capabilities of the OpenFOAM® environment. Starting from an already existing algorithm [24], we undertake all of the steps necessary to expand the range of treatable physical effects. Furthermore, the code is validated against the analytical solution of Young et al. [26] and used to study the impact of the geometrical configuration on the drop migration pattern.

2 Mathematical Formulation

The ingredients of our overall conceptual architecture are provided and discussed in a step-by-step approach, with the aim of defining each of the sub-models as simply as possible and building and growing the framework "organically" by progressive integration of the various components. The class of such sub-parts or sub-models is highly diverse, including typical moving boundary methods and energy transport models in synergy with non-dimensional and asymptotic analyses.

2.1 Governing Equations

We consider the Marangoni migration of a liquid drop surrounded by an immiscible liquid under the effect of a constant temperature gradient $\nabla_\infty T$. The most common way to describe such a flow is based on the consideration of two distinct phases, each with its own set of governing equations, and appropriate interface stress jump conditions to guarantee proper phase coupling (see, e.g., [22]). However, the problem can also be approached in terms of "interface capturing methods", such as the Level Set or the Volume of Fluid. These techniques are based on a different strategy known as the "single-fluid" or "one-fluid" approach (see, e.g., [14], and references therein). The underlying idea is that the system might be considered as if composed of one single fluid with variable material properties (undergoing discontinuities across the fluid–fluid boundaries). In terms of momentum, the presence of the interfacial stresses is accounted for by adding "extra" forces to the transport equation.

More precisely, if we assume that the effect of gravity and any other external body force is negligible, the conservation of momentum can be written as

$$\rho\left(\frac{\partial \mathbf{u}}{\partial t}+\mathbf{u}\cdot\nabla\mathbf{u}\right)=-\nabla p+\nabla\cdot\left[\mu\left(\nabla\mathbf{u}+(\nabla\mathbf{u})^{T}\right)\right]+\mathbf{f}_{\sigma}, \tag{1}$$

where t represents time, ρ, μ are the fluid density and viscosity, respectively, p is the pressure and $\mathbf{u}$ the velocity vector. The last term $\mathbf{f}_{\sigma}$ is a force accounting for the capillary ($\mathbf{f}_{\sigma,\mathbf{n}}$) and thermocapillary ($\mathbf{f}_{\sigma,\tau}$) forces at the interface

$$\mathbf{f}_{\sigma}=\mathbf{f}_{\sigma,n}+\mathbf{f}_{\sigma,\tau}=\sigma(T_0)k\mathbf{n}\delta_{\mathrm{S}}+\nabla_{\|}\sigma(T)\delta_{\mathrm{S}} \tag{2}$$

Here, k and $\mathbf{n}$ are the curvatures and normal unit vector at the interface, respectively, $\mathbf{I}$ is the identity tensor and the operator $\nabla_{\|}=(\mathbf{I}-\mathbf{nn})\nabla$ accounts for the projection of the surface-tension gradient along the direction tangent to the interface. The term δ_{S} represents a distribution function that takes values one at the interface and zero elsewhere [14]. Since the interfacial tension σ depends on the temperature T, we have explicitly included the related dependence in Eq. 2. Closure of the mathematical model requires consideration of the conservation of mass for incompressible flows (Eq. 3) and the temperature transport equation (Eq. 4)

$$\nabla\cdot\mathbf{u}=0, \tag{3}$$

$$\rho c_p\left(\frac{\partial T}{\partial t}+\mathrm{u}\cdot\nabla T\right)=\nabla\cdot(\kappa\nabla T), \tag{4}$$

where c_p is the specific heat and κ the thermal conductivity of the fluid. Following common practice for this kind of problem (see, e.g., [25]), all material properties are assumed to be constant in each phase and are evaluated at a suitable reference temperature. The dependence on temperature, however, is retained for the surface tension σ via a linear relationship

$$\sigma(T)=\sigma_0+\sigma_T(T-T_0), \tag{5}$$

where $\sigma_T=-\partial\sigma(T)\big/\partial T$ is negative for most known fluids [18] and T_0 is the reference temperature.

2.2 The Simplified LS-VOF Method

Our solver relies on a simplified coupled LS-VOF code (based on the hybrid formulation originally developed by Albadawi et al. [1], see also Sussman and Puckett [20]) implemented into the framework of OpenFOAM® [24] as an extension of the standard VOF solver "interFoam". The simplified coupled LS-VOF for an isothermal system is based on the solution of Eqs. 6–10. The equation for the volume fraction reads as

$$\frac{\partial \alpha}{\partial t} + \nabla \cdot (\alpha \mathbf{u}) + \nabla \cdot (\alpha(1-\alpha)\mathbf{u}_c) = 0, \tag{6}$$

where α is the volume fraction and $\mathbf{u}_c$ is an artificial "compressive velocity" [4]. Although there was a consistent improvement in terms of accuracy and reduction of the so-called "parasite" currents with respect to the original two-phase solver, we had to take additional countermeasures to fix typical "algorithm stability" issues at the interface (where Marangoni stresses of thermal nature are produced). This was accomplished by "proper" smoothing, both of the level set and the volume of fluid phase functions, as further described in Sect. 2.3.

The resulting time-marching procedure can be outlined as follows: in order to calculate the level set function φ, we first calculate the field $\varphi_0 = (2\alpha - 1)\Gamma$, where $\Gamma = 0.75\,\Delta x$ and Δx is the grid resolution (see [1]). Subsequently, a re-initialisation equation is solved (see, e.g., [19]):

$$\frac{\partial \varphi}{\partial \tau} = \mathrm{Sgn}(\varphi_0)(1 - |\nabla \varphi|), \tag{7}$$

with the initial condition $\varphi(\mathbf{x}, 0) = \varphi_0(\mathbf{x})$ and where $\mathrm{Sgn}(\varphi_0) = \varphi_0 \big/ |\varphi_0|$ and τ is a fictitious time. Once the scalar field φ is known at each point, it is possible to evaluate the curvature at the interface

$$k(\varphi) = -\nabla \cdot \mathbf{n}(\varphi), \tag{8}$$

with $\mathbf{n}(\varphi) = \nabla\varphi \big/ |\nabla\varphi|$ being the unit vector perpendicular to the interface. Finally, the term described by Eq. 2 is evaluated, leading to the momentum equation cast in compact form as

$$\rho\left(\frac{\partial \mathbf{u}}{\partial t} + \mathbf{u} \cdot \nabla \mathbf{u}\right) = -\nabla p + \nabla \cdot \left[\mu\left(\nabla \mathbf{u} + (\nabla \mathbf{u})^{\mathrm{T}}\right)\right] + \sigma k(\varphi)\eta(\varphi)\nabla\varphi + \sigma_T \nabla_{\parallel} T |\nabla \alpha|, \tag{9}$$

where

$$\eta(\varphi) = \begin{cases} 0 & \text{if } |\varphi| > \varepsilon \\ \frac{1}{2\varepsilon}\left(1 + \cos\left(\frac{\pi\varphi}{\varepsilon}\right)\right) & \text{if } |\varphi| \leq \varepsilon \end{cases} \tag{10}$$

and $2\varepsilon = 3\Delta x$.

The reader is referred to Lappa [14] for additional information about the mathematical manipulations required to turn the surface force seen in Eqs. 1 and 2 into a corresponding volume force spread over a region of finite thickness, which no longer relies on the use of the delta function. Additional details on the dependences on φ and α present in Eq. 9 are provided in Sect. 2.3.

2.3 Implementation of the Thermal Marangoni Migration Method in OpenFOAM®

We used properly mollified variables to increase algorithm stability and avoid non-physical effects at the interface. More precisely, the smoothing was applied to each "relevant variable" χ (various variables required by the LS and VOF implementation in different parts of the solver, as needed) using a "pure diffusive" evolution equation $\chi_{\text{mol}}^{n+1} = \chi_{\text{mol}}^{n} + \left(\nabla^2 \chi_{\text{mol}}^{n}\right)\Delta\tau_{\text{mol}}$, where τ_{mol} represents an artificial or fictitious time, to be solved with the initial condition for a prefixed number of cycles n (the condition $n = 0$ corresponding to the recovery of the original non-smoothed function). $\Delta\tau_{\text{mol}}$ is defined according to the following well-known numerical stability criterion (see, e.g., [8]):

$$\Delta\tau_{\text{mol}} = \frac{0.5^2}{(1/\Delta x)^2 + (1/\Delta y)^2 + (1/\Delta z)^2}. \tag{11}$$

We used mollified quantities to evaluate the new curvature at each time step, i.e.,

$$k_{\varphi\text{mol}} = -\nabla \cdot \mathrm{n}_{\varphi\text{mol}} = -\nabla \cdot \frac{\nabla\varphi_{\text{mol}}}{|\nabla\varphi_{\text{mol}}|}, \tag{12}$$

where φ_{mol} is the smoothed version of φ.

As discussed in Sect. 2.1, accounting for surface-tension effects requires two additional source terms in the momentum equation (see Eq. 2). In the framework of an optimisation strategy based on a trial-and-error approach, we could obtain the best results using the mollified level set function to determine the unit vector perpendicular to the interface (and the corresponding tangent unit vector) and retaining a non-mollified volume fraction in the gradient appearing in the expression of the thermal contribution (see Eq. 13). The level set function was also used accordingly to determine the curvature.

$$\mathbf{f}_{\sigma,\tau} = \sigma_T \nabla_{\parallel} T |\nabla\alpha| = \sigma_T \left(\mathbf{I} - \mathbf{n}_{\varphi\text{mol}}\mathbf{n}_{\varphi\text{mol}}\right)\nabla T |\nabla\alpha|. \tag{13}$$

The portion of the code in which we have included the thermocapillary force is shown in Fig. 1.

Following common practice in the literature [5], the smoothing philosophy has also been applied to the fluid properties (assumed to be constant in each phase) in order to prevent the algorithm from developing spurious oscillations due to the discontinuity established at the liquid–liquid interface. In our hybrid implementation, we decided to rely on a standard VOF approach, expressing each property as

$$\gamma = \alpha_{\text{mol}}\gamma_1 + (1 - \alpha_{\text{mol}})\gamma_2. \tag{14}$$

Special care has also been devoted to the solution of the energy equation. Some mathematical manipulations were indeed necessary to increase algorithm stability

```
fvVectorMatrix UEqn
(
    fvm::ddt(rho, U)
  + fvm::ddt(rhoPhi, U)
  + turbulence->divDevRhoReff(rho, U)
  + ddtSigma*TangentialGradT*mag(fvc::grad(alpha1))
==
    sources(rho, U)
);
```

Fig. 1 Snippet of code from the UEqn.H file. The line highlighted in boldface represents the stresses due to the thermocapillary effect, where ddtSigma represents the interfacial tension coefficient σ_T, `TangentialGradT` is the projection $\nabla_{\|} T$ of the temperature gradient (implemented in the code as `gradT` – (`gradT` & `nMoll`)*`nMoll`, where `gradT` is the temperature gradient and `nMoll` corresponds to $n_{\varphi mol}$) and the last term is the magnitude of the gradient of the volume fraction $|\nabla \alpha|$

```
fvScalarMatrix TEqn
(
    fvm::ddt(T)
  + fvm::ddt(phi, T)
  - fvm::laplacian(D, T)
  - 1.0/(rho*cp)*(fvc::grad(k) & fvc::grad(T))
  + fvc::grad(D) & fvc::grad(T)
);
```

Fig. 2 Implementation of the temperature equation. The name of the variables has direct correspondence to the symbolism adopted in Eq. 15

and its related ability to reproduce available test cases in the literature (as discussed later in this chapter). We rearranged the equation as follows: by introducing the thermal diffusivity $D = \kappa/\rho c_p$ and considering that all the fluid material properties can, in general, change across the interface, after some algebraic manipulations, we obtained the following equivalent expression for the energy equation:

$$\frac{\partial T}{\partial t} + \mathbf{u} \cdot \nabla T = \nabla \cdot (D \nabla T) + \frac{1}{\rho c_p} \nabla \kappa \cdot \nabla T - \nabla D \cdot \nabla T. \tag{15}$$

The snippet of code displayed in Fig. 2 shows the corresponding implementation.

The different macro-steps in which our algorithm has been articulated can ultimately be sketched as follows:

1. Solve the re-initialization equation (Eq. 7);
2. Solve the volume fraction equation using the MULES algorithm (which is essentially an explicit method, see, e.g., the OpenFOAM® user guide [17] to guarantee the boundedness of the scalar field α;
3. Solve the temperature equation;
4. Compute the thermal Marangoni force $\mathbf{f}_{\sigma,\tau}$;
5. Calculate the velocity and pressure field using a projection method (PISO algorithm);
6. Go back to step 1 or end of calculation.

Before the validation and discussion of the results in the next section, we will list here the independent non-dimensional parameters governing the physics of the flow under discussion. These are the fluid property ratios $\widetilde{\rho} = \rho_\mathrm{d}/\rho_\mathrm{m}$, $\widetilde{\mu} = \mu_\mathrm{d}/\mu_\mathrm{m}$, $\tilde{c}_\mathrm{p} = c_{\mathrm{p,d}}/c_{\mathrm{p,m}}$ and $\tilde{k} = k_\mathrm{d}/k_\mathrm{m}$, the Capillary number $Ca = \sigma_T(\nabla_\infty T)R/\sigma_0$, the Marangoni number $Ma = \sigma_T(\nabla_\infty T)R^2/\alpha_\mathrm{m}\mu_\mathrm{m}$ and either the Reynolds number $Re = \rho_\mathrm{m}\sigma_T(\nabla_\infty T)R^2/\mu_\mathrm{m}^2$ or the Prandtl number $Pr = \mu_\mathrm{m}/\rho_\mathrm{m}\alpha_\mathrm{m}$, since $Ma = Re\,Pr$. The subscripts "m" and "d" stand for matrix and drop, respectively.

3 Solver Validation

As indicated at the end of Sect. 2, our overall framework has been built via the integration of self-contained modules, which could be individually tested. However, because it is crucial that the entire numerical architecture be tested as a single integrated unit, we considered available solutions in the literature for comparison. In order to validate our code, in particular, we focused on the thermocapillary motion of a spherical Newtonian droplet of radius R in a constant temperature gradient $\nabla_\infty T$ embedded in an unconfined Newtonian matrix in the limiting case of $(Ma, Re) \to 0$ and negligible buoyancy effects. As discussed in the introduction, in such a case, an analytical solution exists for the velocity of the droplet [26] (YGB theory), which, in dimensional form, reads as

$$U_\mathrm{YGB} = \frac{2|\sigma_T|(\nabla_\infty T)R/\mu_\mathrm{m}}{\left(2+\frac{k_\mathrm{d}}{k_\mathrm{m}}\right)\left(2+3\frac{\mu_\mathrm{d}}{\mu_\mathrm{m}}\right)}, \tag{16}$$

where the temperature gradient $\nabla_\infty T$ is defined as $\nabla_\infty T = (T_\mathrm{hot} - T_\mathrm{cold})/H$, where H is the height of the channel along the direction of the motion (between the hot wall and the cold wall) and T_hot and T_cold correspond to the temperature at the hot wall and cold wall, respectively (cf. Fig. 3a). In our simulations, we assumed conditions corresponding to the following set of (non-dimensional) characteristic numbers: $Pr = 0.1$, $Re = 1.0 \times 10^{-4}$, $Ma = 1.0 \times 10^{-5}$ and $Ca = 2.0 \times 10^{-1}$ (with the capillary number being sufficiently small to guarantee negligible deformations, see, e.g.,

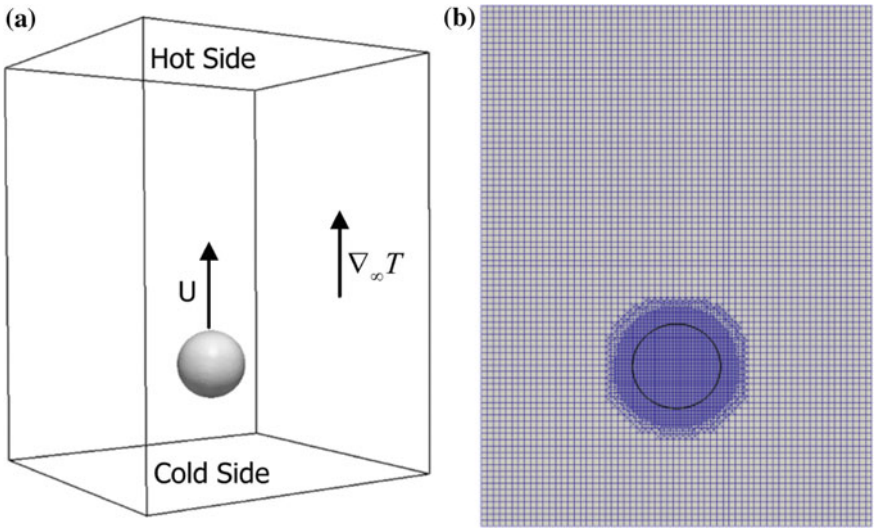

Fig. 3 **a** Initial conditions used for the simulation. At the initial instant, the droplet is at rest. The velocity arrow has been included to show the droplet migration direction when a temperature gradient $\nabla_\infty T$ is imposed. **b** Particular of the mesh in a plane parallel to the motion of the droplet. Note the area of refinement in the region of the droplet

[27]). For simplicity, we also considered the fluid material parameters to be the same for both fluids (i.e., unit fluid property ratios). Assuming the radius of the droplet to be $R = 0.5\,\text{cm}$, we fixed the size of the external container to $(6 \times 4.5 \times 4.5)\,\text{cm}^3$ (shown in Fig. 3a), corresponding to a confinement ratio $C = R/L = 0.22$, where L represents the distance between the centre of the drop and the wall. This size is intended to mimic the effective geometry of the container used in microgravity experiments by Hadland et al. [9]. As shown in Fig. 3b, a structured mesh with $85 \times 64 \times 64$ elements adaptively refined in the region of the drop is employed. For the boundary conditions, we have applied no-slip conditions for the velocity and `"zeroGradient"` for the pressure at each wall of the container (a reference pressure `"pRefValue = 0"` has been set at the centre of the "cold" wall). For the temperature, we set constant values at the "cold" and "hot" sides and adiabatic (`"zeroGradient"`) conditions in the rest of the boundaries of the domain.

All simulations were executed applying two ($n = 2$) cycles of smoothing for the Level Set function φ.

Figure 4 shows a snapshot of the flow pattern and the temperature distribution in a plane parallel to the direction of migration in the case of $C = 0.22$. As expected, a toroidal roll is formed as a result of the thermocapillary effect. The intersection of such a roll with the considered visualisation plane clearly shows regions of recirculating fluid surrounding the droplet. As time increases, such vortices move with the droplet.

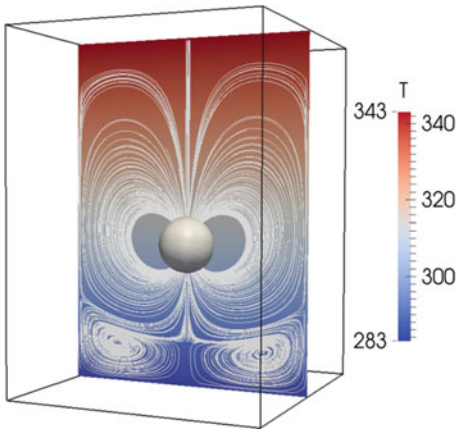

Fig. 4 Snapshot of the flow pattern and temperature field in a plane parallel to the direction of migration at instant $t' = 10$. The droplet is moving from the bottom (cold side) toward the top (hot side)

Figure 5 shows the dimensionless migration velocity as a function of the dimensionless time $t' = \mu_m/\sigma_T(\nabla_\infty T)$ for the same case. As evident in this figure, after a given transient, the droplet reaches a steady state in which its (final) migration velocity is in excellent agreement with the predictions of the YGB theory.

We also studied the effect of the geometric "confinement", considering narrower containers with $C = R/L > 0.22$. We found that the migration velocity decreases nontrivially with the degree of confinement. More specifically, when the height of the geometry is halved ($C = 0.44$), the resulting steady-state migration velocity is about 12% smaller than the limit predicted by the YGB theory. Such results, summarised in Fig. 5, clearly indicate that some care should be taken in the choice of geometry if wall effects are not intended to be a relevant aspect of the analysis.

The last test considered was the simulation of a droplet migrating into a convergent channel, resorting to the same set-up adopted for the previous simulations. We used a convergent duct having a "cold side" cross-sectional area equal to the case of $C = 0.44$, with the cross-sectional area of the "hot side" being half of the cold one.

It is worth emphasising that in such a case, the droplet could not reach a steady state (its velocity increases monotonically, until it suddenly decreases when the droplet is close to the hot wall). Such interesting behaviour, which would require further investigation, might perhaps be explained by the presence of two different counteracting contributions: as the droplet migrates along the converging region, the degree of confinement increases, and on the basis of the previous findings, one should expect the velocity to decrease; however, since the temperature field distribution is no longer linear, and the Marangoni stresses increase accordingly, one should expect the droplet to accelerate. Further studies are in progress along these lines to assess the role played in such dynamics by the relative importance of molecular and inertial transport terms in the governing equations.

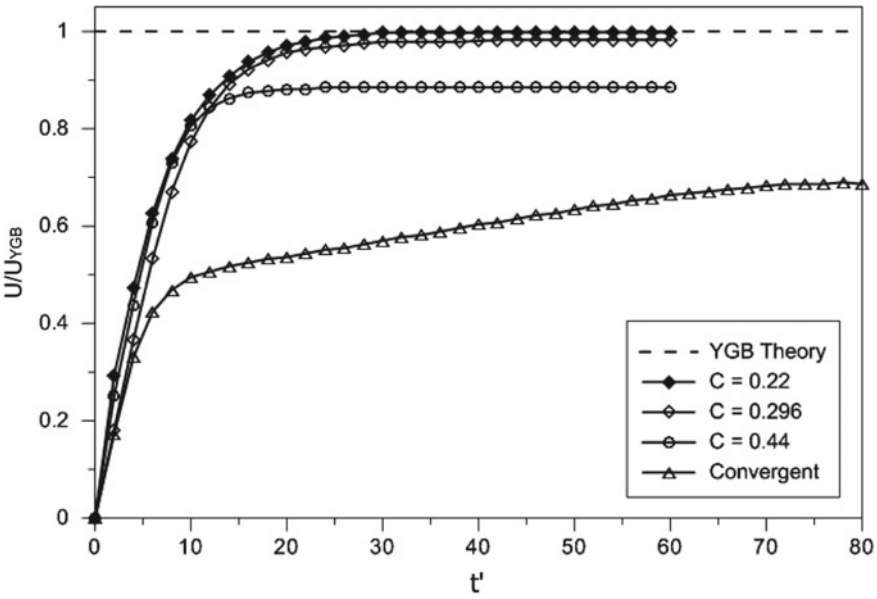

Fig. 5 Velocity history for various geometry and confinements C. The results are normalised using the YGB theoretical velocity. Notice the difference between the two cases $C = 0.296$ (still in good agreement with the YGB theory) and the case $C = 0.44$

4 Conclusions and Future Directions

In this work, we addressed the question of how a typical numerical framework for isothermal multiphase flows can be adequately extended to make it suitable for the simulation of phenomena in which surface-tension gradients act as the main flow or pattern driver. In particular, starting from existing implementations in OpenFOAM® of moving boundary methods, some effort has been put into strengthening the used approach by incorporating the possibility of accounting for thermal effects of different nature in the algorithm. Special care has been devoted to numerical stability issues that are typical of such problems (in which the phenomena occurring in a limited neighbourhood of the interface separating the two liquids play a "crucial role").

The framework has been successfully tested under restricted conditions, but future work shall be devoted to the application and testing of the resulting approach to more complex problems in which inertial terms in the momentum equation and convective-transport terms in the energy equation dominate over the corresponding molecular-transport terms.

References

1. Albadawi A., Donoghue D. B., Robinson A. J., Murray D. B., Delauré Y. M. C., (2013), Influence of surface tension implementation in volume of fluid and coupled Volume of Fluid with Level Set methods for bubble growth and detachment, International Journal of Multiphase Flow, 53, 11–28.
2. Balasubramaniam R. and Subramanian R. S, (2000), The migration of a drop in a uniform temperature gradient at large Marangoni numbers, *Physics of Fluids*, 12(4): 733–743.
3. Balasubramaniam R., Lacy C.E., Wozniak G., Subramanian R.S., (1996), Thermocapillary migration of bubbles and drops at moderate values of the Marangoni number in reduced gravity, *Physics of Fluids*, 8(4): 872–880.
4. Berberović, van Hinsberg N. P., Jarkirlić S., Roisman L. V., Tropea C., (2009), Drop impact onto a liquid layer of finite thickness: Dynamics of the cavity evolution, *Phyical. Review E,* 79, 036306.
5. Brackbill J.U., Kothe D.B., Zemach C., (1992), A Continuum Method for Modeling Surface Tension, *Journal of Computational Physics*, 100 (2): 335–354.
6. Brady P. T., Hermann M., Lopez J. M., (2011), Confined thermocapillary motion of a three-dimensional deformable drop, *Physics of Fluids,* 23, 022101.
7. Brunet P., Baudoin M., Bou Matar O., Zoueshtiagh F., (2010), Droplet displacement an doscillation induced by ultrasonic surface acoustic waves: A quantitative study, *Physical Review E* 81, 036315.
8. Fletcher C. A. J., Compuational techniques for fluid-dynamics (Springer Verlag, Berlin, 1991).
9. Hadland P.H., Balasubramaniam R., Wozniak G., Subramanian R.S., (1999), Thermocapillary migration of bubbles and drops at moderate to large Marangoni number and moderate Reynolds number in reduced gravity, *Experiments in Fluids*, 26: 240–248.
10. Haj-Hariri H., Shi Q., Borhan A., (1997), Thermocapillary motion of deformable drops at finite Reynolds and Marangoni numbers, *Physics of Fluids* 9 (4):845–855.
11. Harper J.F. and Moore D.W., (1968), The motion of a spherical liquid drop at high Reynolds number*, Journal of Fluid Mechanics*, 32(2): 367–391.
12. Lappa M., (2004), Fluids, Materials and Microgravity: Numerical Techniques and Insights into the Physics, 538 pages, Elsevier Science (2004, Oxford, England).
13. Lappa M., (2005a) Assessment of VOF Strategies for the analysis of Marangoni Migration, Collisional Coagulation of Droplets and Thermal wake effects in Metal Alloys under Microgravity conditions, *Computers, Materials & Continua*, 2(1), 51–64.
14. Lappa M., (2005b), Coalescence and non-coalescence phenomena in multi-material problems and dispersed multiphase flows: Part 2, a critical review of CFD approaches, *Fluid Dynamics & Materials Processing*, 1(3): 213–234.
15. Ma X., Balasubramanian R., Subramanian R. S., (1999), Numerical simulation of thermocapillary drop motion with internal circulation, *Numerical Heat Transfer,* 35, 291–309.
16. Nguyen N., Ng K. M., Huang X., (2006), Manipulation of ferrofluid droplet using planar coils, *Applied Physics Letters* 89, 052509.
17. OpenFOAM® User Guide, 2008.
18. Subramanian R. S and Balasubramaniam R., (2001), The motion of bubbles an drops in reduced gravity, *Cambridge University Press.*
19. Sussman, M. and Fatemi, E., (1999): An efficient, interface-Preserving Level Set Redistancing Algorithm and its application to Interfacial Incompressible Fluid Flow. *SIAM Journal of. Scientific Computing*, 20, 1165–1191.
20. Sussman, M., Puckett, E., (2000), A coupled level set and volume-of-fluid method for computing 3D and axisymmetric incompressible two-phase flows. *Journal of Computational Physics*, vol. 162, pp. 301–337.
21. Tryggvason G., Bunner B., Esmaeeli A., Juric D., Al-Rawahi N., Tauber W., Han J., Nas S., and Jan Y.-J., (2001), A Front Tracking Method for the Computations of Multiphase Flow, *Journal of Computational Physics*, 169: 708–759.

22. Tryggvason G., Scardovelli R., Zaleski S., (2011), Direct numerical simulations of gas-liquid multiphase flows, *Cambridge University Press.*
23. Wozniak G., (1991), On the thermocapillary motion of droplets under reduced gravity, *Journal of Colloid and Interface Science*, 141(1): 245–254.
24. Yamamoto T., Okano Y., Dost S., (2016), Validation of the S-CLSVOF method with the density-scaled balanced continuum surface force model in multiphase systems coupled with thermo-capillary flows, *International Journal of Numerical Methods in Fluids*.
25. Yin Z., Chang L., Hu W., Li Q., and Wang H., (2012), Numerical simulations on thermocapillary migrations of nondeformable droplets with large Marangoni numbers, *Physics of Fluids,* 24, 092101.
26. Young N.O., Goldstein J.S., Block M.J., (1959), The motion of bubbles in a vertical temperature gradient*, Journal of Fluid Mechanics*, 6, 350–360.
27. Zhao J., Zhang L., Li Z., Qin W., (2011), Topological structure evolvement of flow and temperature fields in deformable drop marangoni migration in microgravity, *International Journal* of *Heat and Mass Transfer,* 54, 4655–4663.